Massless Fermions in multilayer graphitic systems with misoriented layers.

Sylvain Latil,[1] Vincent Meunier,[2] and Luc Henrard[1]

[1] *Laboratoire de Physique du Solide, Facultés Universitaires Notre-Dame de la Paix, rue de Bruxelles 61, 5000 Namur, Belgium*
[2] *Oak Ridge National Laboratory, Bethel Valley Road, Oak Ridge, TN, 37831-6367, USA*

(Dated: February 1, 2008)

We examine how the misorientation of a few stacked graphene layers affects the electronic structure of carbon nanosystems. We present *ab initio* calculations on bi- and trilayer systems to demonstrate that the massless Fermion behavior typical of single layered graphene is also found in incommensurate multilayered graphitic systems. We also investigate the consequences of this property on experimental fingerprints, such as Raman spectroscopy and scanning tunneling microscopy (STM). Our simulations reveal that STM images of turbostratic few layer graphite are sensitive to the layer arrangement. We also predict that resonant raman signal of graphitic samples are more sensitive to the orientation of the layers than to their number.

PACS numbers: 81.05.Uw, 71.15.Mb, 73.90.+f

The electronic properties of 2D graphene and 3D graphite have been extensively studied for more than 50 years[1]. It is fascinating that the extraordinary properties of carbon nanotubes[2] have been deduced from those of 2D graphene many years before macroscopic samples of very thin Few Layer Graphite (FLG) could be obtained in the laboratory[3]. A particular interest has been recently given to Single Layer Graphene (SLG) because of their massless Fermion behavior, the $\sqrt{B}$ dependence of the Landau levels[4,5], and the observation of abnormal Quantum Hall Effect (QHE), even at room temperature[6].

In that context, a precise investigation of the layer to layer interaction on the existence of massless Fermion carriers is of paramount importance. For 3D graphite, the most stable Bernal phase (AB stacking) as well as the rhombohedral (ABC stacking) have been proven to show complex electron and hole bands near the Fermi level rather than linear, massless fermion ones, due to interlayer interaction[7]. We have recently shown that regular (AB or ABC) stackings also break the linear character of the dispersion of electronic bands for FLG with 2 to 4 layers and that ambipolar electronic conduction could be related to AB stacked FLG[8].

In this Letter, we present an electronic structure analysis of misoriented (turbostratic) 2 and 3 layer FLG. A recent surface X-rays analysis of multilayer graphene grown on SiC shows that misorientation is plausible[9]. We show here that the linear dispersion of SLG is preserved in turbostratic multilayer systems despite the presence of adjacent layers. It follows that massless Fermion carriers are predicted for disoriented multilayer systems. These findings raise the question of the interpretation of the experimental observations performed on FLG samples and challenge the direct relation between SLGs and Dirac massless Fermions. More generally, the electronic properties (and consequently the optical, vibrational, and transport properties) of a given FLG film is found to be controlled mainly by the (mis)orientation of the successive layers rather than the number of layers. In the present work , we discuss also the implications of this possible misorientation on experimental signatures, in particular on STM and Raman fingerprints.

The main technical difficulty when modeling turbostratic structures, is to combine their incommensurate character and the necessary finiteness of the supercell in solid state calculations. An elegant solution, proposed by Kolmogorov and Crespi[10] consists in the definition of a graphene hexagonal supercell without mirror symmetry (except the basal plane). The smallest supercell of this type contains 14 atoms, and is defined with its basis vectors $\mathbf{A}_1 = 2\mathbf{a}_1 + \mathbf{a}_2$ (denoted as $(2,1)$ supercell hereafter) and $\mathbf{A}_2 = -\mathbf{a}_1 + 3\mathbf{a}_2$, as shown on Fig.1. The supercell $(3,\overline{1})$ possesses exactly the same basis vectors, but is rotated by the angle $\cos^{-1}(11/14) \simeq 38.21°$. When stacking these two supercells, we obtain a bilayer structure with short-range incommensurability (Fig.1). The $(7,0)$ and $(5,3)$ supercells also present exactly the same size but a larger number of atoms (98 C atoms per layer), and can be assembled onto bi- or trilayer compounds fulfilling the translational symmetry requirements[11].

In this Letter, we focus our attention on bi- and trilayer FLG structures based on the $(2,1)$ and $(7,0)/(5,3)$ supercells. Our aim is to highlight significant differences in the band structures of commensurate and incommensurate graphitic systems. All the calculations were performed with density functional theory (DFT), within the local density approximation (LDA) scheme[12], and using

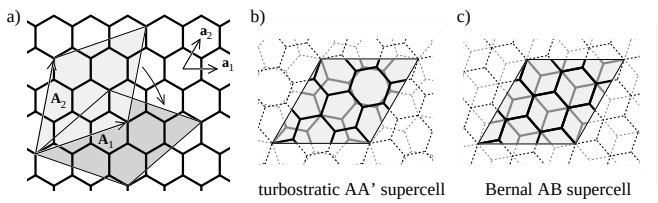

FIG. 1: a) The non-symmetric supercell $(2,1)$ (light grey), and its two primitive vectors $\mathbf{A}_1$ and $\mathbf{A}_2$. The $(3,\overline{1})$ cell is drawn in dark grey. b) A quasi incommensurate bilayer AA' structure, made by stacking the $(2,1)$ on the $(3,\overline{1})$ supercell. c) An AB bilayer structure supercell.

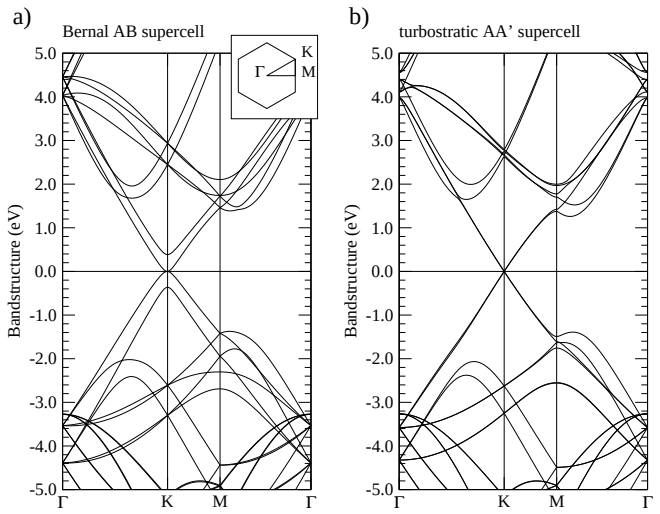

FIG. 2: The 2D electronic band structures of Bernal AB (a) and turbostratic AA' (b) bilayer graphene. Both are based on the supercell represented in Fig. 1. The hexagonal Brillouin zone of the system is shown in the inset.

norm-conserving pseudopotentials[13]. According to the number of atoms involved in the supercell, the eigenproblem was expanded on plane waves (PWs, using the code ABINIT[14]) or localized pseudoatomic orbitals (PAOs, using the code SIESTA[15]). In the first case, plane waves cutoff energy was set to 35 Hartree. In the second case, the basis was composed of atom-centered double-ζ functions.

We carried out a structural optimization of each bilayer $(2,1)$-based supercell (PW calculations with tolerance for the forces set to 10^{-6} Hartree/Bohr and a $12\times12\times1$ grid sampling of the Brillouin zone), prior to the analysis of their electronic structure. No significant atomic rearrangement is observed within a plane, the only structural reorganization taking place in the average inter-layer distance (3.33 Å for the AB, and 3.42 Å for the turbostratic stacked bilayer). The corresponding band structures of the two (2,1)-based bilayers are plotted on Fig. 2. We have carefully verified that PAO basis yields identical results.

Fig. 2a reproduces the well-known results for AB bilayer[8,16] within a supercell $\sqrt{7}\times\sqrt{7}$ larger then the primitive cell and is displayed for comparison. As in previously published calculations, we notice a ~ 0.8 eV splitting of the electronic bands, related to the layer-layer interactions in the AB geometry. The bilayer graphene with a 38.21° misorientation (called AA' hereafter) presents a totally different signature near the Fermi level (Fig.2b). Surprisingly, the band structure here is found to be similar to the one of SLG but doubly degenerate. The significance of this result is striking, since a massless Fermion character is found for misoriented bilayer systems with a Fermi velocity of $\sim 9.6\times10^6$ m s^{-1}, strictly identical to the value deduced for SLG within the same formalism, and similar to experimental values[6,22]. We have checked that this unexpected behavior is also found in the turbostratic $(5,3)$on$(8,\overline{3})$ bilayer that presents a misorientation angle of 43.57°. The apparent absence of interaction between layers at the Fermi level can be related to the loss of short range corrugation between successive layers.

Turning to the trilayer FLG system, we use the interlayer distance found for bilayer cases, depending of the stacking geometry (AB or turbostratic). The PAO electronic calculations shown here have been checked against PW calculations. On Fig.3, we present the results for a purely AA'A" turbostratic $(5,3)$on$(8,\overline{3})$on$(7,0)$ trilayer with two respective misorientations of 43.57° and 38.21°, and for a mixed case $(5,3)$on$(\overline{7},0)$on$(7,0)$, made from a bilayer with AB stacking and a third one misoriented (38.21°), called ABA'. The results for the calculation for ABA or ABC stacking can be found in references[8,17].

The trilayer with a mixed stacking ABA' displays electronic bands (Fig. 3b) similar to a superposition of a AB bilayer (Fig. 2a) and a single-layer graphene (linear dispersion). The band crossing of the graphene-like bands lies 12 meV above the Fermi level, indicating a small charge transfer of $\sim 10^{11}$ e cm^{-2}. The other (quadratic) bands present a gap opening that is consistent with the behavior found for AB bilayer graphene under an electric field[17]. We have checked that the same systems but with the A' layer away from its equilibrium position presents a vanishing small charge transfer, i.e. a progressive closure of the 'gap' of the quadratic bands and a Dirac point of the linear bands moving towards the Fermi level. Interestingly, the turbostratic AA'A" trilayer follows the trends observed for the bilayer and displays linearly dispersive bands and massless Fermion behavior. The (doubly degenerate) bands associated with the external layers are slightly shifted upward ($\sim$12 meV) while the bands related to the central layer are slightly shifted downward($\sim$25 meV). This is also the signature of a small electron transfer, from the external layers to the central one, consistent with the previous ABA' case. We have also checked that the deviation from the linear dispersion of the π-bands for $|E| > 0.5$ eV is mainly due to the trigonal warping effect of graphene and not to an interlayer effect.

The results presented above demonstrate that turbostratic stacking of graphene sheets leads to a linear dispersion of the electronic levels similar to the behavior of SLG. Furthermore, the mixed stacking case shows a superposition of the two types of carriers, i.e. a massless Fermion and a massive, normal electronic behavior. Consequently, direct experimental evidence of Dirac Fermion behavior can no longer be considered as a discriminating property between single and multilayered systems. In particular, the number of π bands in Angle resolved photoemission spectroscopy (ARPES) measurement[18] is not a definitive evidence of the number of layers but should be cross-checked with other experimental techniques.

The absence of a net effect of interlayer interaction on the electronic dispersion of turbostratic FLG also suggests that the $\sqrt{B}$ dependence of the Landau levels will

also occur for multilayer structures and that the abnormal QHE cannot be excluded. Remarkably, this consequence of our study is supported by recent experimental data. First, $\sqrt{B}$ Landau level separation have been observed in 3-5 graphene layers[5]. Second, Dirac Fermion behavior, integer QHE[19] and infrared probe anomalous magnetotransport have been also reported in a Highly Ordered Pyrolytic Graphite (HOPG) bulk 3D sample[20]. Third, the unconventional QHE has been reported on bilayer graphene[21], challenging the common interpretation in terms of AB stacking. Finally, other studies[22] relate the coexistence of two types of carriers (Dirac Fermion and normal electron) in HOPG bulk graphite, consistent with the findings presented herein.

Recently, the observation of a single 2D band (~ 2700 cm^{-1}) in Raman spectroscopy has been proposed as an experimental tool for the determination of the number of layers in FLG samples[16,23,24]. For two-layer (and thicker) films, the interlayer interaction induces a splitting of the electronic bands. This means that in a double resonance Raman process, the resulting effect is a splitting of this $2D$ peak[16,24]. Our results show that the effect of the interlayer interaction on the splitting of the electronic bands crucially depends on the relative orientation of the layers. For instance, since a turbostratic bilayer possesses degenerate electronic bands near the Fermi level, the $2D$ mode of this structure gives rise to a single peak that is indistinguishable from the signature of SLG systems. Similarly, a trilayer turbostratic structure will also present a single $2D$ band. Indeed, as we have discussed above, the splitting of the electronic bands in that case is due to a charge transfer and no evidence of covalent mixing has been found. The $2D$ peak of the mixed ABA' trilayer will present three main features. Two of them are associated with the AB-like bands, the third one with the A' layer, identical to the SLG case.

Interestingly, the splitting of the $2D$ band of graphitic materials has been found to be a good criteria of crystallinity perpendicular to the basal planes. For instance, in Ref. 25, the authors have correlated the interlayer distance in bulk graphite with the doubling of the $2D$ band and they found that for $d > 0.338$ nm a single $2D$ band is observed where a double $2D$ band is observed for $d < 0.338$ nm. From these findings and the results presented here, we can propose that HOPG graphite with disorder in the staking (and large d) will present a single $2D$ line whereas Bernal graphite with (partial) AB order will present a doubling of the $2D$ line. ¿From this discussion, it is clear that a unequivocal determination of the number of layers is not possible from Raman spectroscopy alone.

We now analyse the STM images of the trilayer systems studied above. Recent experimental data on mono- and bilayer graphite on SiC substrate show a $\sqrt{3} \times \sqrt{3}$ modulation of the STM intensity. This effect has been associated with the substrate reconstruction[26,27,28] rather than to the relative arrangement of the graphitic layers. Here, we have computed the STM images of trilayer systems without the substrate in order to discriminate the intrinsic response of FLG from the effect of interaction with the substrate. This approach is made possible by the prerequisite of Tersoff-Hamann theory since the image formation is governerd by integration of local density of states, and does not require a closed circuit to simulate the current[29]. Here we made use of the BSKAN package implementation of Tersoff-Hamann[30,31]. Constant current images for systems represented in Fig. 3 are shown in Fig. 4 for positive and negative tip polarities. For system ABA' the two external faces are not equivalent and the corresponding images are given for both faces. At

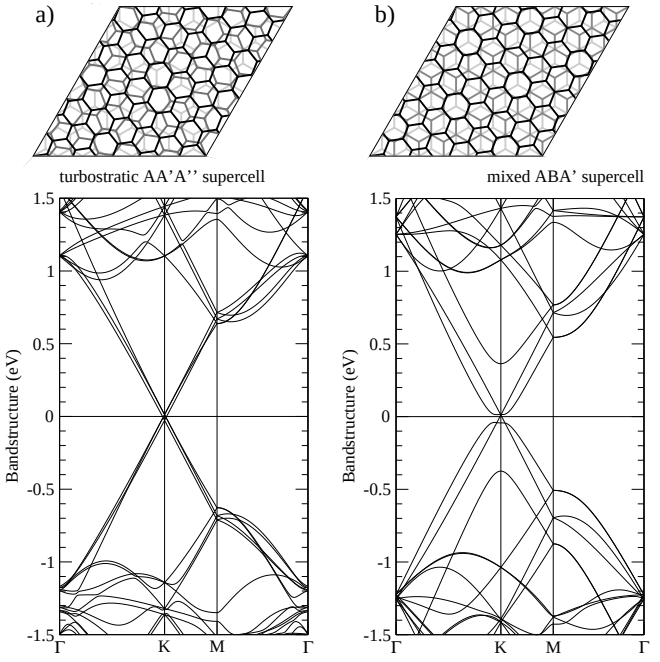

FIG. 3: Representation of the supercells and the correponding electronic band structure for trilayer graphites. The turbostratic AA'A" system (43.57° and 38.21° misorientation angles) is shown in (a), and the mixed ABA' structure is shown in (b).

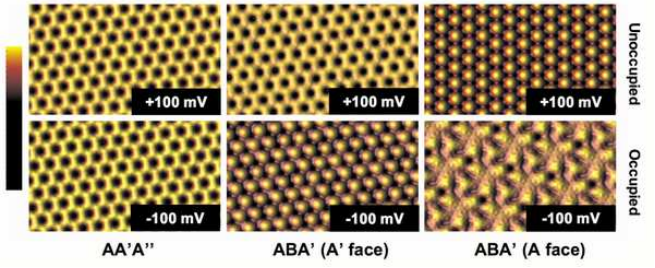

FIG. 4: (color online) ¿From left to right: constant current STM image simulation of turbostratic AA'A" and mixed ABA' systems. (Un)occupied states are images at (positive) negative tip potential. The color scale spans the corrugation of each system: 1.6 (1.4) Å, 2.3 (2.4) Å, and 1.8 (2.1) Å for each system at positive (negative) bias.

low bias (100 meV was used here), the images reflect the property of the states close to the Fermi level. For system AA'A"', both positive and negative bias images look the same, with all the atoms being imaged, just as in SLG. The situation is quite different for ABA' systems. The image for occupied states of the A' face shows bright spots on every other atom, while a complete honeycomb lattice is imaged for unoccupied states. The situation is even more complicated for images computed on the A face of the ABA' system. While every other atom is now revealed at tip bias corresponding to unoccupied states, the occupied state image clearly shows a small-scale Moiré-like pattern. It is important to note that the images have been simulated for zero temperature conditions: given the very small energy difference between the states responsibles for the images at low bias, the room temperature image will most probably look like an average of the images reproduced here.

In summary, we have performed *ab initio* calculations of the electronic band structures of misoriented (turbostratic) FLG. We surprisingly found that, as a consequence of the incommensurability of the layers, such multilayer systems possess a massless Fermion carriers property. Since that property was up to now considered as a unique signature of single layer graphene, the present findings challenge the interpretation of the experimental data on FLG. They also release the restriction to SLG sample to build devices based on massless fermion physics.

Calculations were performed at the Namur Interuniversity Scientific Computing Facility (I-SCF), a common project between the FRS-FNRS and the University of Namur. S.L. and L.H. acknowledge the financial support from the Belgian FNRS. V.M. acknowledges the Division of Materials Sciences, US Department of Energy, under Contract No. DEAAC05-00OR22725 with UT Battelle, LLC at ORNL.

[1] J. W. McClure, Phys. Rev. **108**, 612 (1957); J. C. Slonczewski and P. R. Weiss, ibid **109**, 272 (1958).
[2] J.-C. Charlier, X. Blase, and S. Roche, Rev. Mod. Phys. **79**, 677 (2007).
[3] K. S. Novoselov *et al.*, Science **306**, 666 (2004); C. Berger *et al.*, J. Phys. Chem. B **108**, 19912 (2004).
[4] V. P. Gusynin and S. G. Sharapov, Phys. Rev. B **73**, 245411 (2006).
[5] M. L. Sadowski *et al.*, Phys. Rev. Lett. **97**, 266405 (2006).
[6] K. S. Novoselov *et al.*, Nature **438**, 197 (2005); V. P. Gusynin and S. G. Sharapov, Phys. Rev. Lett. **95**, 146801 (2005); Y. Zhang, Y.-W. Tan, H. L. Stormer, and P. Kim, Nature **438**, 201 (2005); K. S. Novoselov *et al.*, Science **315**, 1379 (2007).
[7] J.-C. Charlier, X. Gonze, and J.-P. Michenaud, Phys. Rev. B **43**, 4579 (1991); Carbon **92**, 289 (1994).
[8] S. Latil and L. Henrard, Phys. Rev. Lett. **97**, 036803 (2006).
[9] J. Hass *et al.*, cond-mat/0702540.
[10] A. N. Kolmogorov and V. H. Crespi, Phys. Rev. B **71**, 235415 (2005).
[11] It is impossible to create a totally misoriented trilayer structure based on the (2,1) supercell, that is still compatible with the translationnal symmetry requirements.
[12] S. Goedecker, M. Teter, and J. Hutter, Phys. Rev. B **54**, 1703 (1996).
[13] N. Troullier and J. L. Martins, Phys. Rev. B **43**, 8861 (1991).
[14] X. Gonze *et al.*, Computational Materials Science **25**, 478 (2002).
[15] J. M. Soler *et al.*, J. Phys.: Condens. Matter **14**, 2745 (2002).
[16] D. Graf *et al.*, Nanolett. **7**, 238 (2007).
[17] M. Aoki and H. Amawashi, Solid State Comm. **142**, 123 (2007).
[18] T. Ohta *et al.*, Science **313**, 951 (2006); T. Ohta *et al.*, Phys. Rev. Lett. **98**, 206802 (2007); A. Bostwick *et al.*, Nature Phys. **3**, 36 (2007).
[19] H. Kempa, P. Esquinazi, and Y. Kopelevich, Solid State Comm. **138**, 118 (2006).
[20] Z. Q. Li *et al.*, Phys. Rev. B **74**, 195404 (2006); G. Li and E. Y. Andrei, Nature Phys. **3**, 623 (2007).
[21] K. S. Novoselov *et al.*, Nature Phys. **2**, 177 (2006).
[22] I. A. Luk'yanchuk and Y. Kopelevich, Phys. Rev. Lett. **97**, 256801 (2006); S. Y. Zhou *et al.*, Nature Phys. **2**, 595 (2007).
[23] A. Gupta *et al.*, Nanolett. **6**, 2667 (2006).
[24] A. C. Ferrari *et al.*, Phys. Rev. Lett. **97**, 187401 (2006).
[25] P. Lespade, A. Marchand, M. Couzi, and F. Cruege, Carbon **22**, 375 (1984).
[26] P. Mallet *et al.*, cond-mat/0702406.
[27] G. Rutter *et al.*, Solid State Comm. **142**, 123 (2007).
[28] F. Varchon *et al.*, cond-mat/0702311.
[29] J. Tersoff and D. R. Hamann, Phys. Rev. B 31, 805 (1985).
[30] W. A. Hofer and J. Redinger, Surf. Sci. Rep. 447, 51 (2000).
[31] For convenience, the DFT charge density used for STM simulation were obtained using the plane-wave VASP package (G. Kresse and J. Hafner, Phys. Rev. B 47, 558 (1993); G. Kresse and J. Furthmuller, Comput. Mater. Sci. 6, 15 (1996); Phys. Rev. B 54, 11169 (1996).), which can be readily used for STM simulations. The sames parameters for VASP as for ABINIT calculations were used as described in the text, yielding to identical results.